Journal of Chemical&Engineering Data

pubs.acs.org/jced

Article

H_2, N_2, CO_2, and CH_4 Unary Adsorption Isotherm Measurements at Low and High Pressures on Zeolitic Imidazolate Framework ZIF-8

Junyoung Hwang, Hassan Azzan, Ronny Pini, and Camille Petit*

Cite This: https://doi.org/10.1021/acs.jced.1c00900

Read Online

ACCESS | Metrics & More | Article Recommendations | Supporting Information

ABSTRACT: Excess adsorption of CO_2, CH_4, N_2, and H_2 on ZIF-8 was measured gravimetrically in the pressure range ranging from vacuum to 30 MPa at 298.15, 313.15, 333.15, 353.15, and 394.15 K using a magnetic suspension balance. The textural properties of the adsorbent material—i.e., skeletal density, surface area, pore volume, and pore-size distribution—were estimated by helium gravimetry and N_2 (77 K) physisorption. The adsorption isotherms were fitted with the Sips isotherm model and the virial equation, and the values of isosteric heat of adsorption and Henry constants for the gases were determined using the latter.

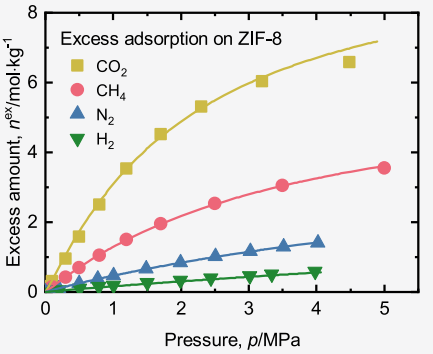

INTRODUCTION

Adsorption technologies have been developed and employed for gas separation and purification in applications such as carbon capture and natural gas processing.[1] For instance, in the precombustion capture from steam methane reforming, a high-pressure mixture of H_2 and CO_2 is produced as a reaction effluent containing small amounts of impurities such as CH_4, N_2, CO, and Ar.[2] Here, one can use adsorption to remove these impurities and coproduce CO_2 (for sequestration) and H_2 (as a low carbon fuel or as a raw material for the chemical industry). For CH_4 purification in natural gas processing, impurities such as N_2 and CO_2 need to be removed from "raw" natural gas prior to commercial supply to avoid instances of equipment and pipeline corrosion, and unwanted emissions.[3]

In the above cases, as in any other separation in which adsorption is envisioned, knowledge of adsorption equilibrium of the respective gas mixtures, on a given adsorbent, at the relevant process pressure and temperature conditions is a prerequisite to developing an adsorption-based process.[1] For a pressure swing (PSA) or vacuum swing adsorption (VSA) process, adsorption data are necessary within the pressure range from vacuum up to the feed partial pressures of the gases in the feed mixture at minimum.[4] These data sets allow accurate prediction of the adsorption behavior at higher pressures using an isotherm model without introducing any error due to extrapolation. Similarly, the temperature conditions of the adsorption data must encompass the entire range of temperatures that may be present in the process. This is particularly important for temperature swing adsorption (TSA) processes where large changes in temperature drive the separation.[5] Ideally, one would collect multicomponent equilibrium data for the targeted gas mixtures to model the separation accurately. Yet, generating mixture adsorption data remains uncommon as it requires a purpose-made setup that is capable of analyzing the composition of the gas mixture of the feed and of the bulk after the system has reached equilibrium. To circumvent this challenge, one can predict multicomponent adsorption equilibria using theories such as ideal adsorbed solution theory (IAST) or model them using semiempirical isotherm models, such as extended Langmuir or Sips models based on pure component adsorption isotherm data.[6−9]

Within the types of adsorbent, zeolitic imidazolate frameworks (ZIFs) are a subgroup of metal−organic frameworks. ZIFs display a zeolitic topology arising from the coordination between transition metal ions and imidazolate ligands. Their structural features, such as large surface area and high porosity, coupled with their chemical and thermal stability[10,11] have attracted much attention for the applications of gas storage and separations.[12−16] ZIF-8 represents one of the most studied ZIF members owing to its easy synthesis, stability, and pore aperture size which is well suited for the adsorption of small gas molecules like the ones involved in precombustion CO_2 capture and natural gas processing.

In this work, we collected unary adsorption isotherm data for a commercially available ZIF-8 over a wide range of temperatures and pressures relevant to processes such as

Special Issue: Equilibrium Adsorption Data for Energy and Environmental Applications

Received: November 30, 2021
Accepted: February 14, 2022

precombustion CO_2 capture and natural gas processing. More specifically, we present gravimetrically measured adsorption of CO_2 (up to 30 MPa), CH_4 (up to 25 MPa), N_2 (up to 4 MPa), and H_2 (up to 4 MPa) in the temperature range from 298.15 to 393.15 K. We modeled the equilibrium behaviors of these adsorption systems using the Sips isotherm model and the virial equation. In presenting the adsorption data, we have rigorously demonstrated measurement reproducibility and highlighted sources of uncertainty. By doing so, this study provides a reliable set of reference adsorption isotherms for multiple gases at different temperatures on a commercially available adsorbent.

EXPERIMENTS

Materials and Gases. Table 1 lists the details of the adsorbent material and pure gases used in this work. The adsorbent material and sourced gases, CO_2, CH_4, and N_2, were used as-received without further purification. H_2 was generated using deionized water (resistivity of 18.2 MΩ × cm) with a PEAK Scientific Precision Hydrogen 100 H_2 Generator that is capable of producing H_2 at a purity of up to 99.9995% and a maximum pressure of 0.8 MPa. The generator is connected to a Maximator DLE 5-1-2 GG Hydrogen Gas Booster which uses an air drive at a pressure up to 1 MPa to compress the H_2 produced from the generator, that can be supplied at a maximum pressure of 0.8 MPa. A constant N_2 purge is used during compression to prevent the mixing of high pressure H_2 and air, as shown in Figure 1. Powder ZIF-8 sample (particle size = 4.9 μm as indicated by the supplier, powder X-ray diffraction measurements are shown in Figure S1) was activated for over 12 h under continuous vacuum (4×10^{-4} mbar) at 473.15 K prior to performing adsorption measurements of CO_2 and CH_4, while 393.15 K was used to activate the sample prior to N_2 and H_2 adsorption measurements. The two temperature conditions are above the activation temperature of 373.15 K suggested by the supplier (Aldrich) and within the reported realm of thermal stability of ZIF-8.[10] Thermogravimetric analysis curves support activation temperature of 473.15 K, when guest molecules are removed from the ZIF-8 structure.[17−19] However, the difference in the two activation temperatures did not have a significant effect on the experimental reproducibility as discussed later.

Table 1. Details of the Adsorbent Material and Gases Employed in This Study, As Provided by the Manufacturer/Supplier

name	CAS number	source	purity [%]
2-methylimidazole zinc salt (ZIF-8, Basolite Z1200)	59061-53-9	Aldrich	≤100
carbon dioxide (CO_2)	124-38-9	BOC	99.995
methane (CH_4)	74-82-8	BOC	99.995
nitrogen (N_2)	7727-37-9	BOC	99.999 2
hydrogen (H_2)	1333-74-0	PEAK Scientific	99.999 5
helium (He)	7440-59-7	BOC	99.999

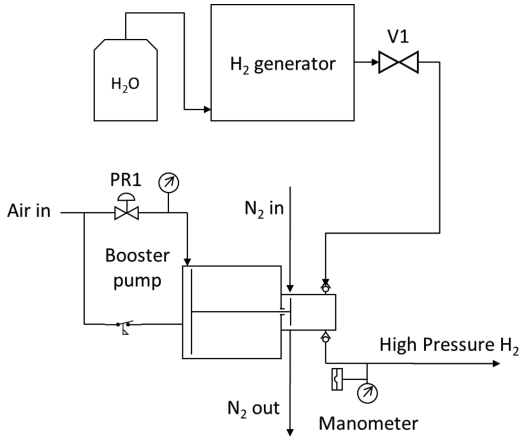

Figure 1. Schematic of the setup used to produce high purity H_2 at high pressure.

Determination of Textural Parameters. The textural parameters of ZIF-8 were derived from the N_2 physisorption measurements at 77 K, performed using Autosorb iQ (Quantachrome Instruments) in the pressure range of 1.5×10^{-7} to 0.1 MPa. The sample was activated *ex situ* at 473.15 K under continuous vacuum for 12 h prior to the physisorption measurements. The experiment was conducted twice using separate aliquots to test experimental repeatability (see Figure S2 for the repeated measurements). Only the latter run was used for further analysis. The surface area, pore volume, and pore-size distribution (PSD) of ZIF-8 were determined by fitting the N_2 adsorption branch with the nonlocal density functional theory (NLDFT) model (cylindrical/spherical on silica/zeolite) supplied by Quantachrome Instruments with its proprietary data analysis software (ASiQwin). The fitting error of the NLDFT model was 8.64%.

Equilibrium Sorption Measurements. The high-pressure adsorption measurements have been conducted using a gravimetric sorption analyzer with a Rubotherm magnetic suspension balance (IsoSORP HPII). The details of the setup, including its schematic diagram, have been described in our previous work.[20] The setup shown in Figure S1 of Hwang and Pini[20] was modified to supply H_2 into the measuring chamber by integrating a H_2 generator as shown in Figure 1. The purity of the generated H_2 was ensured by regenerating the silica desiccant in the built-in drying column of the gas generator prior to experimental measurements to achieve the maximum purity quoted by the manufacturer (99.9995%). Furthermore, the density of the bulk H_2 was measured *in situ* by the suspension balance and compared to the density values calculated using an appropriate equation of state[21] obtained from REFPROP.[22] The agreement between the measured and calculated density of H_2 indicates that the gas generated by the setup is relatively free from impurities (see Figure S3).

The adsorbed quantities measured by the suspension balance are excess and net amounts of adsorption. The suspension balance reads weight measurements (resolution of 10 μg) at two measuring positions: MP_1, which is the weight of the adsorbent plus the suspended metal parts, and MP_2, which is MP_1 plus a titanium sinker (known volume). The following equations apply with these two weight measurements:

$$m^{ex} = MP_1 - MP_{1,0} + \rho_b V_0 \quad (1)$$

$$m^{net} = MP_1 - MP_{1,0} + \rho_b V_{met} \quad (2)$$

$$\rho_b = \frac{(MP_{2,0} - MP_{1,0}) - (MP_2 - MP_1)}{V_{sk}} \quad (3)$$

https://doi.org/10.1021/acs.jced.1c00900
J. Chem. Eng. Data XXXX, XXX, XXX−XXX

where the subscript 0 indicates weight measurements taken under vacuum; m^{ex} and m^{net} are excess and net adsorbed amounts in mass, respectively; ρ_b is the bulk fluid density; V_{met}, V_0, and V_{sk} are the volumes of the suspended metal parts, V_{met} plus the adsorbent volume (V_s), and of the titanium sinker, respectively. While V_{sk} is known (4.364 cm^3), V_{met} and V_0 are estimated by introducing CO_2 without a sample (making the left-hand side of eq 2 equal to zero) as shown in Figure S1 of Pini et al.[23] and introducing He with a sample loaded under the assumption that He is nonadsorbing (making the left-hand side of eq 1 equal to zero), respectively. To increase accuracy, these measurements are carried out at several pressure points, so as to cover the pressure range probed experimentally. The value of V_{met} used in this study has been obtained from measurements conducted with CO_2 at 353.15 K from vacuum to 30 MPa, while the value of V_0 has been obtained from measurements conducted with He at 393.15 K from vacuum to 30 MPa. The resulting value of V_0 can then be used to determine the skeletal density of the adsorbent:

$$\rho_s = m_s/(V_0 - V_{met}) \tag{4}$$

Finally, m^{ex} and m^{net} are reported in specific molar basis (n^{ex} and n^{net}, respectively) in this study by dividing them by the molecular weight, M, and sample mass, m_s.

The adsorption isotherms were measured by increasing the pressure starting from a vacuum state (a minimum pressure of 4×10^{-4} mbar) and reaching an equilibrium condition at a fixed temperature. The adsorption system was left to reach equilibrium for at least 60 min until the weight change in the last 15 min was below 100 μg. Overnight ($\geq$12 h) measurements were regularly conducted to confirm that no significant amounts of adsorption occur past the usual equilibration time. After confirming equilibrium, the average of the last five measurements was used to calculate the adsorption amount at the given pressure and temperature conditions. We estimated the values of uncertainty based on the general formula of error propagation, the summary of which is included in the Supporting Information.

To confirm the reproducibility and repeatability of the measurements produced by the setup, CO_2 adsorption isotherm measurements were repeated using two separate aliquots at two temperatures, 333.15 and 353.15 K, as shown in Figure 2. The repeated data sets show good agreement at both temperatures and between the two aliquots. These two aliquots were prepared and activated at two separate instances by two different researchers. Such practice complies with the standards proposed by Han et al.[24] to enhance experimental reproducibility. Furthermore, the difference in the two activation temperatures between the two aliquots (473.15 and 393.15 K, respectively) did not have a significant effect on the experimental reproducibility. The measurement accuracy of the setup has been further demonstrated by reproducing the reference isotherms (generated by fitting multiple interlaboratory data sets) presented by the National Institute of Standards and Technology (NIST) in its interlaboratory studies[25,26] for two adsorption systems: CO_2/ZSM-5 (293.15 K) and CH_4/zeolite Y (298.15 K). For both adsorption systems, all of our adsorption measurements fell within the uncertainty intervals (0.075 mol/kg and 0.09 mol/kg for CO_2 and CH_4, respectively) of the reference isotherms (see Figure S4).

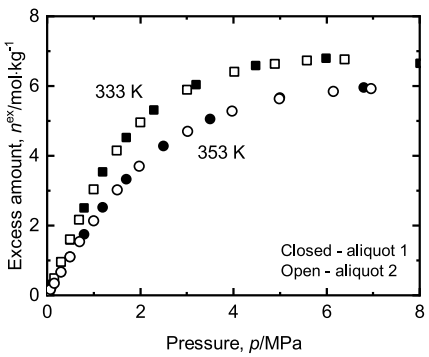

Figure 2. Repeated CO_2 adsorption isotherms using two ZIF-8 sample aliquots at 333.15 K (squares) and 353.15 K (circles).

Equilibrium Isotherm Modeling. The equilibrium data were fitted to the empirical Sips isotherm model, which is given by the following equations:[27]

$$n_i^* = n_{s,i}\frac{(k_i p)^{1/m_i}}{1 + (k_i p)^{1/m_i}} \tag{5}$$

$$k_i = k_i^0 \exp\left(\frac{Q_i}{RT}\right) \tag{6}$$

For a pure component i, n_i^* is the absolute amount of gas adsorbed, $n_{s,i}$ is the saturation capacity, k_i is the adsorption coefficient, described by an expression with two constants, k_i^0 which is the pre-exponential factor, and Q_i which is the characteristic energy of k_i, and m_i is a constant heterogeneity parameter. We did not consider the estimated conversion of the measured excess adsorbed quantities to absolute adsorbed quantities in this work. Therefore, in our analysis we only included data measured at bulk gas densities, ρ_b^m, below 10% of the liquid adsorbate densities at the lowest temperature conditions (ρ_a = 1179, 422, 808, and 71 kg/m^3 for CO_2, CH_4, N_2, and H_2, respectively). Mathematically

$$n^{ex} = n^*\left(1 - \frac{\rho_b^m}{\rho_a}\right) \approx n^* \tag{7}$$

While we took into account all N_2 and H_2 data points based on this criterion, we truncated CO_2 and CH_4 data points below 4.7 and 6.3 MPa, respectively. As an example of general validity, taking 0.55 cm^3/g as the micropore volume of ZIF-8 (Table 2), the differences between n^{ex} and n^* for CO_2 at 298 K are 3.3% at 0.2 MPa and 3.8% at 1 MPa. The largest difference at the highest-pressure condition (4 MPa) is 12.5%; however, we argue that conversion to absolute poses additional problems for partially mesoporous materials as in the case of ZIF-8 as discussed in Pini et al.[23]

Table 2. Structural Properties of ZIF-8 Derived from N_2 Sorption Isotherms at 77 K

material	surface area [m^2/g]	pore volume [cm^3/g]	microporosity [%]
ZIF-8	1690	0.64	86

Fitting of the equilibrium data to the Sips model was done by employing a maximum likelihood estimator (MLE). The objective function for the MLE is given as follows:

https://doi.org/10.1021/acs.jced.1c00900
J. Chem. Eng. Data XXXX, XXX, XXX−XXX

$$J(\boldsymbol{\theta}) = \frac{N_t}{2}\ln\left(\sum_{j=1}^{N_t}(n^*_{i,j,\mathrm{exp}} - n^*_{i,j,\mathrm{calc}}(\boldsymbol{\theta}))^2\right) \quad (8)$$

N_t is the total number of data points for pure component i at all temperatures, $n^*_{i,j,\mathrm{exp}}$ is the experimentally determined value of the absolute amount adsorbed at a given p and T, and $n^*_{i,j,\mathrm{calc}}(\boldsymbol{\theta})$ is the calculated value of the absolute amount adsorbed at the same p and T for a set of isotherm parameters given by the vector $\boldsymbol{\theta}$. The objective function is minimized using the built-in MATLAB function *global search*, an algorithm that repeatedly runs a local solver (in this case fmincon) within the bounds set for the parameters to obtain the global optimal values of the parameter vector θ. The resulting vector of optimal parameters is given by $\boldsymbol{\theta}^*$.

The uncertainty bounds at a given confidence interval for the estimated parameters with respect to the experimental data was determined upon approximating the covariance matrix of the estimated parameter vector $\boldsymbol{\theta}^*$ as follows:[28]

$$\boldsymbol{V}_o = \sigma^2\left(\sum_{j=1}^{N_t}\left(\frac{\partial n^*_{i,j,\mathrm{calc}}(\boldsymbol{\theta}^*)}{\partial\boldsymbol{\theta}}\right)\left(\frac{\partial n^*_{i,j,\mathrm{calc}}(\boldsymbol{\theta}^*)}{\partial\boldsymbol{\theta}}\right)^T\right)^{-1} \quad (9)$$

where σ is the standard deviation of the model with respect to the experimental data given by

$$\sigma = \sqrt{\frac{1}{N_t - N_p}\sum_{j=1}^{N_t}(n^*_{i,j,\mathrm{exp}} - n^*_{i,j,\mathrm{calc}}(\boldsymbol{\theta}^*))^2} \quad (10)$$

Here, N_p is the number of parameters in $\boldsymbol{\theta}^*$. $\partial n^*_{i,j,\mathrm{calc}}(\boldsymbol{\theta}^*)/\partial\boldsymbol{\theta}$ is the sensitivity matrix of the model predicted adsorbed amount with respect to the parameter vector $\boldsymbol{\theta}$. Using this, the independent confidence intervals for $\boldsymbol{\theta}^*$ can be obtained at a probability η, as follows:

$$\delta\boldsymbol{\theta}^* = |\boldsymbol{\theta}^* - \boldsymbol{\theta}| = \sqrt{\frac{F^{-1}_{\chi^2}(\eta, N_p)}{\mathrm{diag}(\boldsymbol{V}_o^{-1})}} \quad (11)$$

Here, $F^{-1}_{\chi^2}(\eta, N_p)$ is the inverse of the chi-squared cumulative distribution function with N_p degrees of freedom, evaluated at the probability η obtained using the MATLAB function chi2inv. The uncertainty in the parameter estimates with respect to the experimental data in this work were obtained at 95% confidence. The fitting and uncertainty analysis was implemented using an in-house script developed using MATLAB R2020a (The Mathworks Inc.).

As can be seen from eq 5, the Sips isotherm model does not reduce to the Henry's Law in the limit of low pressure ($p \to 0$). Therefore, the Henry constant, K_H, and the isosteric heat of adsorption, ΔH, were determined from the virial equation, which provides reliable estimates of K_H from high-pressure adsorption isotherms, in which the Henry's region may be difficult to identify.[27,29] The virial equation is given by the following equation[30,31] for each component i:

$$\ln(p/n_i^*) = \frac{1}{T}\sum_{j=0}^{M_1} a_j n_i^* + \sum_{j=0}^{M_2} b_j n_i^* \quad (12)$$

where a and b are characteristic virial coefficients for a gas–solid system. In this study, we used $M_1 = 3$ and $M_2 = 1$ to provide a good fit. The Henry constant can be approximated from a_0 and b_0 using the following equation:

$$K_H = \exp\left(-\frac{a_0}{T} - b_0\right) \quad (13)$$

and the isosteric heat of adsorption is calculated using the following equation:[30,31]

$$\Delta H = -R\sum_{j=0}^{M_1} a_j n_i^* \quad (14)$$

The equilibrium data were fitted to the virial equation and the uncertainty bounds were calculated using the same procedure described above.

RESULTS AND DISCUSSION

Textural Characterization. We first focus on the characterization of the ZIF-8 sample, namely its skeletal density and porosity. The adsorbent skeletal volume is necessary to calculate the excess amount of adsorption as previously discussed. To this end, measurements with He are performed under the assumption that this exposure of the adsorbent to this gas leads to negligible adsorption. In this study, we conducted multiple sets of He measurements at 393.15 K. The pressure ranges of the measurements can be seen in Table S1. The sets of weight measurements are shown in Figure 3. While the different sets of measurements shown in

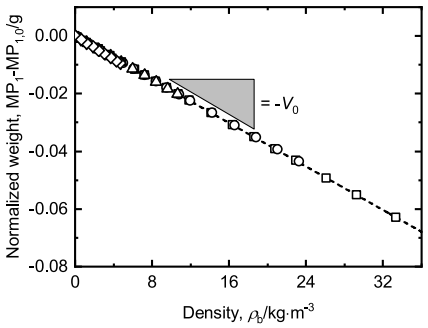

Figure 3. Normalized weight ($MP_1 - MP_{1,0}$) plotted against He density measured at 393.15 K. The slope of the linear regression line is equivalent to the negative value of $V_0 = V_s + V_{met}$. Different symbols represent repeated experiments.

Figure 3 seem to outline a single line, the estimated values of V_0 show a significant level of variation (relative variation of 2%). The corresponding values of ρ_s are summarized in Table 3 and also demonstrates a moderate level of agreement among literature data obtained from various experimental and computational studies. Such differences in the repeated measurements of ρ_s result in noticeable differences in the calculated values of excess adsorption at high pressures. The discrepancy is especially large for dense gases such as CO_2. For instance, the maximum (1.520 g/cm^3) and minimum (1.439 g/cm^3) values in Table 3 result in over 50% difference in the excess adsorbed amounts at 30 MPa (see Figure S5). The difficulty in determining ρ_s partly stems from the assumption that He does not adsorb, which has been questioned for highly microporous solids even at high temperatures.[32−35] In this study, we chose ρ_s = 1.518 g/cm^3 to compute the excess adsorption amounts. At the same time, we report both excess and net adsorption data to provide the readers the freedom to use their own estimated value of ρ_s.

Figure 4 shows the physisorption isotherms of N_2 at 77 K, and Table 2 summarizes the surface area, pore volume, and

https://doi.org/10.1021/acs.jced.1c00900
J. Chem. Eng. Data XXXX, XXX, XXX−XXX

Table 3. Skeletal Density of ZIF-8 Compared to the Literature Values Obtained via Experimental and Computational Methods[a]

ref	method	remark	skeletal density [g/cm^3]
this study	experimental	run 1	1.462 (0.004)
		run 2	1.518 (0.003)
		run 3	1.520 (0.005)
		run 4	1.494 (0.002)
		run 5	1.439 (0.003)
Nguyen et al.[36]	experimental	activated	1.482 (0.002)
		nonactivated	1.501 (0.004)
	computational	activated	1.50
Zhou et al.[37]	experimental		1.4
	computational		1.3
Voskuilen et al.[38]	experimental		1.4 (0.4)

[a]The values in parentheses represent the uncertainty values.

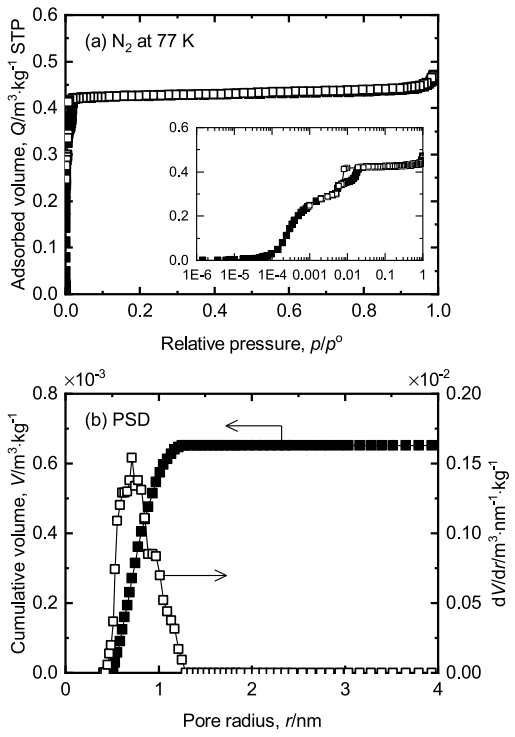

Figure 4. (a) N_2 adsorption (closed symbols) and desorption (open symbols) isotherms on ZIF-8 at 77 K and (b) cumulative volume (left *y*-axis) and PSD (right *y*-axis) obtained from the NLDFT model. (a, inset) Measurements plotted in logarithmic scale.

PSD derived using the NLDFT model. The isotherms conform to the Type 1 classification[39] typical of microporous materials, such as ZIF as demonstrated by the PSD in Figure 4b. The step increase in the isotherms shown in the inset plot of Figure 4a has been previously documented and attributed to the expansion of organic linkers.[40−42] The surface area and pore volume obtained in this study are toward the upper limit of the range provided by the supplier (surface area of 1300−1800 m^2/g) and that of the reported values in the literature.[10,38,40,43−45]

CO_2 and CH_4 Adsorption Isotherms up to 30 MPa. We report the excess adsorption isotherms of CO_2 (298.15, 313.15, 333.15, 353.15, and 393.15 K) and CH_4 (313.15, 333.15, and 353.15 K) on ZIF-8 in Figure 5. From the

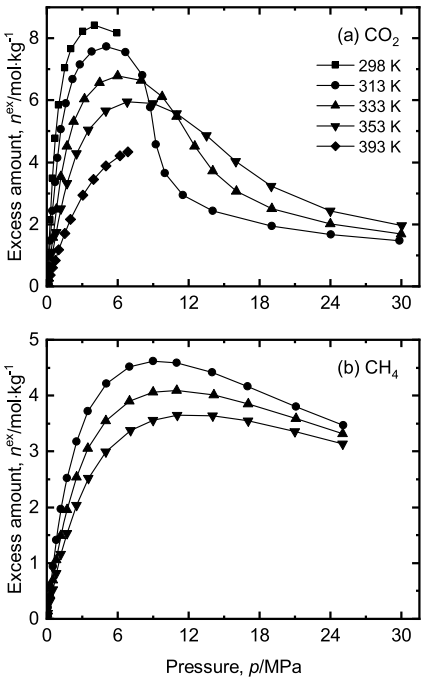

Figure 5. Excess adsorption isotherms of (a) CO_2 and (b) CH_4 on ZIF-8 at various temperatures. The error bars have been omitted for visual clarity as the upper and lower bounds of uncertainty fell within the size of the markers. The lines are added to guide the eye.

repeated CO_2 adsorption measurements, we only present here the data sets with broader pressure ranges. The data sets are given in Tables 4, 5, 6, and 7 with uncertainty values associated with each adsorption point. The adsorption isotherms of both CO_2 and CH_4 at all temperatures (with an exception of the CO_2 at 393.15 K due to the limited pressure range) show monotonic increase until reaching maximum points, between 4 to 7 MPa for CO_2 (within 298.15 to 353.15 K) and 9 to 11 MPa for CH_4 (within 313.15 to 353.15 K). We can interpret the locations of these maximum points by plotting isotherms as a function of density (see Figure S6). When compared to the density value where the increase in density occurs, the locations of maximum appear at lower values of density. This phenomenon is especially visible for CO_2, due to the filling of the micropores. Such saturation of micropores at low density values allows the adsorbed volume to be estimated from the micropore volume, from which approximation of the absolute amounts of adsorption is possible.[23] However, such practice is outside the scope of this study, and we report here only the measured quantities of excess and net adsorption. Furthermore, we observe crossing of the CO_2 isotherms after reaching the excess maximum when plotted as a function of pressure, consistent with previous observations on other porous media.[46,47] We attribute such observation to the rapidly increasing CO_2 density of the bulk phase at lower temperatures.[23,48] Therefore, we do not see the same effect in the isotherms of CH_4, the bulk density of which does not show a sharp increase at the same temperatures, and the crossing of CO_2 isotherms also disappears when plotted as a function of density.

CO_2, CH_4, N_2, and H_2 Adsorption Isotherms up to 4 MPa. We present the excess adsorption isotherms of CO_2, CH_4, N_2 (298.15, 333.15, 353.15 and 393.15 K), and H_2 (298.15, 333.15, 353.15, and 393.15 K) on ZIF-8 in Figure 6

https://doi.org/10.1021/acs.jced.1c00900
J. Chem. Eng. Data XXXX, XXX, XXX−XXX

Table 4. Excess and Net Adsorbed Amounts of CO_2 on ZIF-8 at Different Temperatures and the Uncertainty Values Associated with Them Denoted by δ

pressure [MPa]	density [kg/m^3]	n^{ex}	n^{net}	δn^{ex}	δn^{net}
		298.15 K	[mol/kg]		
0.020	0.378	0.137	0.131	0.003	0.003
0.044	0.816	0.299	0.286	0.002	0.002
0.070	1.283	0.476	0.456	0.004	0.004
0.150	2.704	1.025	0.985	0.002	0.002
0.302	5.463	2.139	2.058	0.003	0.002
0.491	8.955	3.486	3.352	0.002	0.001
0.712	13.137	4.766	4.570	0.004	0.004
0.982	18.380	5.844	5.569	0.004	0.004
1.519	29.319	7.043	6.604	0.005	0.004
2.039	40.667	7.655	7.047	0.020	0.020
3.027	64.746	8.217	7.248	0.005	0.002
4.052	95.241	8.419	6.993	0.013	0.011
5.928	185.085	8.174	5.404	0.026	0.023
		313.15 K			
0.024	0.425	0.114	0.108	0.002	0.001
0.056	0.967	0.263	0.249	0.002	0.001
0.101	1.724	0.475	0.449	0.002	0.001
0.302	5.169	1.461	1.384	0.003	0.002
0.498	8.603	2.437	2.308	0.004	0.004
0.701	12.215	3.365	3.182	0.005	0.005
0.901	15.823	4.145	3.908	0.006	0.006
1.200	21.369	5.056	4.736	0.008	0.007
1.600	29.048	5.900	5.465	0.009	0.008
2.198	41.143	6.678	6.062	0.010	0.009
2.801	54.199	7.146	6.335	0.011	0.009
3.802	78.515	7.564	6.388	0.012	0.010
5.054	114.604	7.731	6.016	0.013	0.009
6.650	177.737	7.550	4.890	0.014	0.009
8.112	285.035	6.802	2.536	0.018	0.008
8.759	393.081	5.767	−0.116	0.022	0.011
9.249	514.477	4.578	−3.122	0.027	0.014
10.014	615.428	3.651	−5.560	0.031	0.016
11.505	694.950	2.938	−7.463	0.035	0.019
14.016	758.131	2.430	−8.917	0.038	0.022
19.027	826.198	1.933	−10.432	0.041	0.024
24.013	869.714	1.669	−11.348	0.043	0.025
29.858	906.786	1.475	−12.097	0.045	0.027
		333.15 K Run 1			
0.019	0.305	0.062	0.057	0.002	0.001
0.047	0.742	0.147	0.136	0.002	0.001
0.068	1.068	0.212	0.196	0.002	0.001
0.153	2.436	0.483	0.446	0.001	0.001
0.301	4.812	0.954	0.882	0.002	0.001
0.501	8.061	1.591	1.470	0.002	0.002
0.688	11.146	2.165	1.998	0.002	0.002
1.000	16.412	3.038	2.792	0.002	0.001
1.496	25.023	4.142	3.767	0.002	0.001
2.004	34.212	4.945	4.433	0.005	0.005
3.007	53.517	5.894	5.093	0.004	0.003
4.028	75.335	6.403	5.275	0.005	0.002
4.892	95.548	6.630	5.200	0.007	0.003
5.578	113.103	6.721	5.028	0.008	0.003
6.399	136.194	6.750	4.712	0.022	0.020
		333.15 K Run 2			
0.020	0.338	0.064	0.059	0.002	0.001
0.052	0.841	0.163	0.150	0.002	0.001
0.100	1.599	0.312	0.288	0.002	0.001
0.300	4.811	0.946	0.874	0.003	0.002
0.500	8.070	1.582	1.461	0.003	0.003
0.801	13.064	2.494	2.298	0.004	0.004
1.199	19.841	3.530	3.233	0.005	0.005
1.701	28.695	4.516	4.087	0.007	0.006
2.299	39.696	5.308	4.714	0.008	0.007
3.199	57.372	6.040	5.181	0.010	0.008
4.487	85.799	6.577	5.293	0.011	0.008
5.999	124.522	6.787	4.923	0.012	0.008
8.015	191.021	6.638	3.779	0.014	0.008
9.757	272.547	6.120	2.041	0.016	0.007
11.014	352.006	5.476	0.208	0.019	0.008
12.507	461.571	4.517	−2.392	0.025	0.013
14.018	551.790	3.725	−4.533	0.028	0.014
16.019	630.532	3.070	−6.367	0.032	0.018
19.010	701.661	2.512	−7.990	0.035	0.020
23.997	772.637	2.016	−9.548	0.038	0.022
29.997	827.074	1.682	−10.697	0.041	0.024
		353.15 K Run 1			
0.020	0.302	0.048	0.043	0.002	0.002
0.047	0.697	0.105	0.095	0.001	0.001
0.069	1.038	0.156	0.140	0.003	0.003
0.152	2.275	0.336	0.302	0.002	0.001
0.297	4.466	0.656	0.590	0.003	0.003
0.498	7.557	1.096	0.983	0.005	0.005
0.701	10.687	1.530	1.370	0.005	0.004
1.002	15.394	2.134	1.903	0.002	0.001
1.505	23.481	3.014	2.662	0.002	0.002
1.987	31.480	3.691	3.219	0.004	0.003
3.019	49.411	4.693	3.953	0.007	0.006
3.977	67.557	5.267	4.256	0.005	0.002
4.990	87.912	5.624	4.308	0.006	0.002
6.149	113.192	5.835	4.140	0.010	0.006
6.962	132.848	5.913	3.924	0.012	0.009
		353.15 K Run 2			
0.021	0.320	0.048	0.044	0.002	0.002
0.055	0.842	0.125	0.113	0.002	0.002
0.101	1.522	0.224	0.201	0.002	0.002
0.301	4.545	0.664	0.596	0.002	0.002
0.499	7.569	1.099	0.986	0.002	0.002
0.800	12.244	1.734	1.551	0.003	0.003
1.201	18.584	2.509	2.231	0.004	0.003
1.700	26.709	3.320	2.920	0.005	0.005
2.498	40.248	4.278	3.675	0.007	0.006
3.509	58.602	5.051	4.174	0.008	0.007
4.999	88.028	5.660	4.342	0.010	0.007
6.804	128.661	5.944	4.019	0.011	0.007
9.013	188.640	5.896	3.073	0.013	0.006
11.004	255.313	5.569	1.748	0.015	0.006
13.494	356.107	4.859	−0.471	0.019	0.008
15.999	461.405	4.020	−2.886	0.024	0.011
19.000	562.315	3.222	−5.194	0.028	0.015
23.999	667.226	2.439	−7.547	0.033	0.018
30.003	742.213	1.952	−9.156	0.037	0.022
		393.15 K			
0.027	0.355	0.036	0.031	0.002	0.001
0.049	0.642	0.061	0.052	0.002	0.001

https://doi.org/10.1021/acs.jced.1c00900
J. Chem. Eng. Data XXXX, XXX, XXX−XXX

Table 4. continued

pressure [MPa]	density [kg/m^3]	n^{ex}	n^{net}	δn^{ex}	δn^{net}	pressure [MPa]	density [kg/m^3]	n^{ex}	n^{net}	δn^{ex}	δn^{net}
		393.15 K	[mol/kg]					393.15 K	[mol/kg]		
0.068	0.912	0.087	0.073	0.002	0.002	2.007	28.029	2.167	1.748	0.002	0.001
0.152	2.035	0.187	0.157	0.002	0.002	3.025	43.148	2.937	2.292	0.003	0.001
0.296	3.994	0.362	0.303	0.002	0.001	3.941	57.482	3.457	2.596	0.004	0.002
0.496	6.716	0.600	0.500	0.002	0.002	5.007	74.702	3.891	2.773	0.005	0.002
0.705	9.590	0.843	0.699	0.002	0.001	6.190	94.741	4.218	2.800	0.007	0.003
1.004	13.721	1.179	0.973	0.003	0.002	6.841	106.347	4.336	2.745	0.008	0.003
1.503	20.770	1.700	1.389	0.002	0.002						

Table 5. Excess and Net Adsorbed Amounts of CH_4 on ZIF-8 at Different Temperatures and the Uncertainty Values Associated with Them Denoted by δ

pressure [MPa]	density [kg/m^3]	n^{ex}	n^{net}	δn^{ex}	δn^{net}	pressure [MPa]	density [kg/m^3]	n^{ex}	n^{net}	δn^{ex}	δn^{net}
		313.15 K	[mol/kg]					333.15 K	[mol/kg]		
0.022	0.133	0.040	0.034	0.004	0.003	3.497	21.049	3.053	2.188	0.007	0.005
0.051	0.319	0.100	0.086	0.004	0.003	5.004	30.558	3.552	2.298	0.007	0.005
0.102	0.628	0.199	0.173	0.004	0.003	7.008	43.540	3.906	2.118	0.009	0.005
0.300	1.859	0.578	0.502	0.004	0.003	9.006	56.816	4.060	1.727	0.009	0.005
0.501	3.104	0.933	0.806	0.004	0.003	10.999	70.333	4.094	1.206	0.011	0.006
0.800	4.983	1.416	1.211	0.005	0.004	14.128	91.406	4.015	0.261	0.012	0.007
1.199	7.505	1.963	1.655	0.005	0.004	17.013	110.319	3.854	−0.676	0.014	0.008
1.704	10.747	2.525	2.084	0.006	0.004	21.081	135.313	3.584	−1.972	0.016	0.010
2.501	15.946	3.176	2.521	0.006	0.005	25.016	156.972	3.314	−3.132	0.018	0.011
3.492	22.644	3.721	2.791	0.007	0.005			353.15 K			
5.022	33.183	4.212	2.849	0.008	0.006	0.021	0.118	0.015	0.011	0.006	0.005
7.000	47.398	4.515	2.568	0.009	0.006	0.050	0.272	0.045	0.034	0.004	0.003
9.006	62.344	4.613	2.052	0.010	0.006	0.101	0.550	0.106	0.083	0.004	0.003
11.001	77.575	4.585	1.399	0.011	0.006	0.301	1.644	0.318	0.250	0.005	0.004
13.987	100.380	4.415	0.293	0.013	0.007	0.500	2.743	0.522	0.409	0.007	0.007
16.995	122.610	4.164	−0.871	0.015	0.008	0.799	4.401	0.812	0.631	0.006	0.006
21.081	150.231	3.798	−2.372	0.017	0.010	1.198	6.609	1.157	0.885	0.006	0.006
25.093	173.708	3.466	−3.668	0.020	0.013	1.698	9.400	1.537	1.151	0.005	0.004
		333.15 K				2.500	13.934	2.034	1.462	0.006	0.004
0.023	0.132	0.029	0.024	0.004	0.004	3.532	19.890	2.520	1.703	0.008	0.007
0.053	0.308	0.076	0.064	0.004	0.003	5.014	28.520	2.993	1.822	0.007	0.005
0.103	0.593	0.146	0.121	0.004	0.004	7.068	40.710	3.378	1.706	0.009	0.007
0.301	1.742	0.424	0.353	0.004	0.003	9.004	52.505	3.562	1.406	0.010	0.007
0.501	2.918	0.694	0.574	0.007	0.006	11.033	64.841	3.648	0.985	0.010	0.006
0.799	4.653	1.056	0.865	0.005	0.004	14.015	82.918	3.643	0.238	0.011	0.006
1.200	7.029	1.495	1.206	0.005	0.004	17.025	100.735	3.546	−0.590	0.013	0.008
1.707	10.050	1.958	1.546	0.006	0.006	20.987	122.994	3.356	−1.695	0.014	0.009
2.504	14.879	2.537	1.926	0.006	0.004	25.032	143.773	3.131	−2.774	0.016	0.010

with the Sips isotherm fitting. The adsorption capacity of ZIF-8 shows a decreasing trend for these gases in the following order: CO_2 > CH_4 > N_2 > H_2. The model parameters are summarized in Table 8. As mentioned above, we did not consider the conversion of excess adsorption to absolute adsorption here and we fitted the isotherms up to medium pressures for CO_2 and CH_4.[49,50] The Sips empirical isotherm model allows a better fit for adsorbents that exhibit weak adsorbent−adsorbate interactions and represents a combination of Langmuir and Freundlich behaviors. This model results in an initially convex shape at low pressures, and a leveling off at higher pressures due to the material exhibiting high microporosity as seen in the experimental data for CO_2.[27] Adsorption isotherms of CO_2, CH_4, and N_2 isotherms show a very good fit to the Sips isotherm model, and the error in the measurement is within the Sips model uncertainty. On the other hand, H_2 isotherms appear to show considerably more noise. This is due to the gravimetric measurement coupled with the low adsorption capacity for H_2 and the low molecular weight of the gas (2.02 g/mol). For these reasons, uncertainty in the experimental data is noticeably larger when compared to the other gases. However, the uncertainty in these experimental data points, when reported in g/g, is in the same order of magnitude for all gases. The data was fitted to the Sips isotherm model for all gases as the heterogeneity factor is necessary to allow a good fit at low pressures for CO_2, and the same model was used for the other gases for consistency.

We characterized the adsorbate−adsorbent interactions using two metrics: the Henry constant and heat of adsorption.

https://doi.org/10.1021/acs.jced.1c00900
J. Chem. Eng. Data XXXX, XXX, XXX−XXX

Table 6. Excess and Net Adsorbed Amounts of N_2 on ZIF-8 at Different Temperatures and the Uncertainty Values Associated with Them Denoted by δ

pressure [MPa]	density [kg/m^3]	n^{ex}	n^{net}	δn^{ex}	δn^{net}
		298.15 K	[mol/kg]		
0.053	0.579	0.042	0.029	0.002	0.001
0.200	2.245	0.163	0.111	0.002	0.002
0.496	5.584	0.392	0.260	0.003	0.003
0.797	9.001	0.607	0.395	0.002	0.002
0.993	11.221	0.735	0.471	0.002	0.002
1.497	16.933	1.037	0.639	0.003	0.002
2.003	22.670	1.300	0.767	0.003	0.002
2.479	28.071	1.513	0.853	0.003	0.002
3.020	34.210	1.725	0.921	0.004	0.002
3.508	39.936	1.900	0.961	0.004	0.002
4.019	45.780	2.055	0.979	0.005	0.003
		333.15 K			
0.054	0.477	0.021	0.010	0.002	0.001
0.204	1.978	0.097	0.051	0.002	0.002
0.496	4.933	0.239	0.123	0.002	0.002
0.773	7.728	0.366	0.185	0.006	0.005
1.003	10.037	0.465	0.229	0.005	0.005
1.488	14.926	0.661	0.310	0.004	0.003
1.996	20.049	0.846	0.374	0.003	0.002
2.510	25.206	1.012	0.419	0.004	0.003
3.021	30.324	1.160	0.447	0.004	0.003
3.519	35.458	1.294	0.460	0.004	0.002
4.024	40.491	1.408	0.456	0.005	0.003
		353.15 K			
0.050	0.492	0.020	0.008	0.003	0.002
0.205	1.965	0.081	0.035	0.004	0.004
0.506	4.819	0.196	0.082	0.004	0.004
0.682	6.491	0.261	0.109	0.010	0.010
0.992	9.432	0.369	0.148	0.003	0.002
1.502	14.267	0.536	0.201	0.003	0.002
1.997	18.951	0.684	0.238	0.003	0.002
2.505	23.743	0.820	0.262	0.009	0.008
3.014	28.520	0.945	0.274	0.004	0.003
3.540	33.607	1.066	0.275	0.004	0.003
4.013	38.044	1.161	0.267	0.005	0.004
		393.15 K			
0.042	0.360	0.006	−0.003	0.006	0.006
0.198	1.693	0.049	0.009	0.003	0.003
0.500	4.262	0.124	0.024	0.011	0.011
0.784	6.677	0.191	0.034	0.003	0.003
1.010	8.600	0.246	0.043	0.004	0.004
1.514	12.875	0.357	0.054	0.004	0.004
2.011	17.069	0.455	0.054	0.012	0.012
2.505	21.243	0.550	0.051	0.005	0.004
3.018	25.549	0.643	0.043	0.007	0.006
3.501	29.715	0.723	0.024	0.008	0.007
4.013	33.942	0.796	−0.002	0.004	0.002

Table 7. Excess and Net Adsorbed Amounts of H_2 on ZIF-8 at Different Temperatures and the Uncertainty Values Associated with Them Denoted by δ

pressure [MPa]	density [kg/m^3]	n^{ex}	n^{net}	δn^{ex}	δn^{net}
		298.15 K	[mol/kg]		
0.209	0.173	0.100	0.043	0.077	0.075
0.488	0.401	0.180	0.049	0.027	0.020
0.806	0.661	0.254	0.038	0.027	0.020
1.012	0.830	0.310	0.038	0.029	0.022
1.467	1.198	0.403	0.012	0.039	0.034
2.009	1.640	0.523	−0.013	0.028	0.021
2.510	2.043	0.620	−0.047	0.028	0.021
3.007	2.436	0.710	−0.086	0.043	0.039
3.526	2.857	0.801	−0.132	0.075	0.073
4.033	3.257	0.883	−0.181	0.028	0.021
		333.15 K			
0.204	0.158	0.063	0.012	0.028	0.020
0.505	0.385	0.115	−0.011	0.028	0.021
0.789	0.596	0.161	−0.033	0.028	0.021
1.003	0.752	0.197	−0.049	0.027	0.020
1.504	1.122	0.270	−0.097	0.029	0.022
1.993	1.481	0.343	−0.141	0.029	0.022
2.445	1.816	0.397	−0.196	0.033	0.027
3.017	2.230	0.474	−0.254	0.030	0.024
3.341	2.473	0.511	−0.297	0.028	0.020
3.981	2.932	0.594	−0.364	0.027	0.020
		353.15 K			
0.044	0.027	0.000	−0.009	0.033	0.027
0.201	0.133	0.010	−0.034	0.028	0.021
0.505	0.340	0.047	−0.064	0.031	0.025
0.805	0.547	0.085	−0.094	0.057	0.054
0.959	0.654	0.101	−0.113	0.039	0.034
1.517	1.034	0.160	−0.178	0.029	0.022
1.876	1.275	0.194	−0.223	0.029	0.022
2.497	1.694	0.250	−0.303	0.030	0.023
3.011	2.040	0.299	−0.367	0.035	0.029
3.516	2.382	0.348	−0.430	0.034	0.028
4.065	2.745	0.383	−0.514	0.033	0.027
		393.15 K			
0.052	0.037	−0.002	−0.014	0.033	0.027
0.206	0.128	−0.002	−0.044	0.028	0.021
0.500	0.310	0.042	−0.059	0.031	0.025
0.794	0.491	0.063	−0.098	0.057	0.054
0.975	0.599	0.081	−0.115	0.039	0.034
1.454	0.902	0.110	−0.185	0.029	0.022
1.999	1.240	0.175	−0.230	0.029	0.022
2.443	1.510	0.177	−0.316	0.030	0.023
3.005	1.837	0.208	−0.392	0.035	0.029
3.490	2.136	0.233	−0.465	0.034	0.028
4.093	2.507	0.275	−0.544	0.033	0.027

Table 9 summarizes the values of K_H determined using the virial equation (the isotherm fits and virial coefficients are summarized in the Supporting Information; see Figure S7 and Table S2). The values of K_H follow the same order as the adsorption capacity for the gases, and K_H values for CO_2 are significantly greater than those of other gases at all temperatures, indicating high selectivity toward CO_2. The heat of adsorption was calculated as a function of loading using the virial isotherm fits obtained using the method described previously, as opposed to using the experimentally determined data. Figure 7 shows the dependence of ΔH on the loading amount where the y-intercept represents the value at zero coverage, ΔH_0. ΔH_0 decreases in the order: CO_2 > CH_4 > H_2 > N_2. In contrast to K_H, the value of ΔH_0 for CO_2 is close to those of CH_4 and H_2. The values of ΔH_0 are greater than the latent heat of vaporization, ΔH_v: 10.3, 8.2, 6.1, and 0.9 kJ/mol for CO_2 (at 273 K), CH_4 (at 112 K), N_2 (at 78 K), and H_2 (at 20 K), respectively.[51,52] While the ratio $\Delta H_0/\Delta H_v$ for CO_2,

https://doi.org/10.1021/acs.jced.1c00900
J. Chem. Eng. Data XXXX, XXX, XXX−XXX

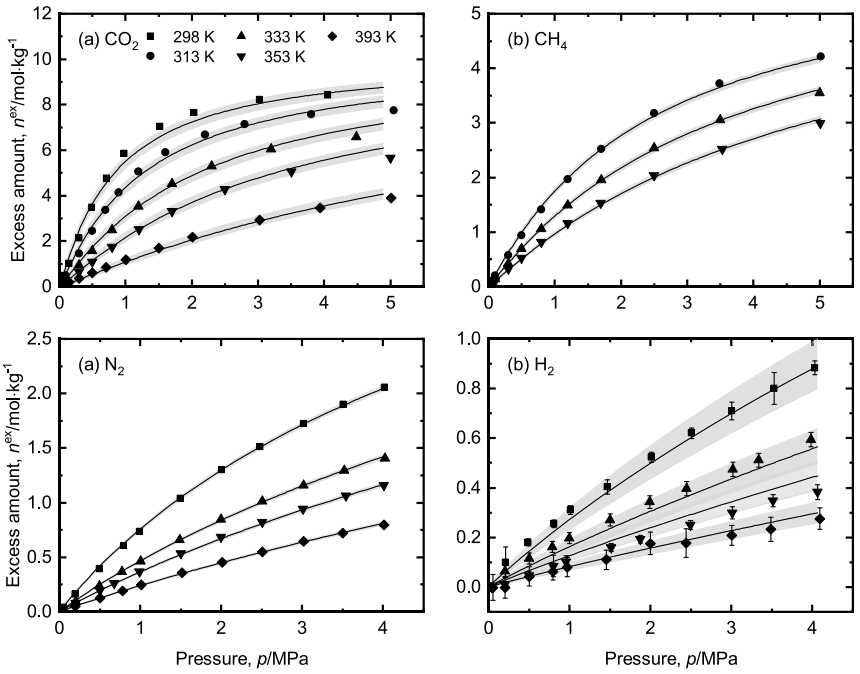

Figure 6. Excess adsorption isotherms of (a) CO_2, (b) CH_4, (c) N_2, and (d) H_2 on ZIF-8 at different temperatures. The error bars for CO_2, CH_4, and N_2 have been omitted for visual clarity as the upper and lower bounds of uncertainty fell within the size of the markers. The solid lines represent the Sips isotherm fitting results, and the shaded regions show the uncertainty bounds of the fitting results.

Table 8. Sips Isotherm Model Parameters Derived from Fitting the CO_2, CH_4, N_2, and H_2 isotherms[a]

fluid	n_s [mol/kg]	$k^0 \times 10^4$ [MPa^{-1}]	Q [kJ/mol]	$1/m$ [−]
CO_2	10.04 (0.22)	1.87 (0.09)	21.71 (0.12)	1.09 (0.06)
CH_4	6.15 (0.05)	6.56 (0.10)	16.78 (0.03)	1.04 (0.02)
N_2	5.18 (0.03)	7.24 (0.06)	13.39 (0.02)	0.96 (0.01)
H_2	4.72 (0.28)	2.52 (0.18)	13.27 (0.19)	0.95 (0.03)

[a]The values in parentheses represent the uncertainty values.

Table 9. Henry Constants Determined from the Zeroth-Order Virial Coefficients: a_0 and b_0[a]

temperature [K]	K_{H,CO_2}	K_{H,CH_4}	K_{H,N_2}	K_{H,H_2}
	[mol/kg · MPa]			
298.15	7.10 (0.37)		0.78 (0.05)	0.33 (0.04)
313.15	5.02 (0.25)	1.95 (0.12)		
333.15	3.32 (0.16)	1.36 (0.08)	0.45 (0.03)	0.17 (0.02)
353.15	2.30 (0.11)	0.98 (0.06)	0.35 (0.02)	0.13 (0.01)
393.15	1.23 (0.06)		0.22 (0.01)	0.07 (0.01)

[a]The values in parentheses represent the uncertainty values.

CH_4, and N_2 conform to the general relation $\Delta H_0/\Delta H_v < 1.5-2$,[53] ΔH_0 is much greater than that of ΔH_v for H_2. Furthermore, we observe an increasing trend for ΔH of CO_2, in contrast to that of CH_4, which can be attributed to the intermolecular attractive forces.[54] The trends of ΔH of N_2 and H_2 stay relatively constant as loading increases.

PERSPECTIVES ON THE MEASUREMENTS

Literature Comparison. As indicated earlier, ZIF-8 is one of the most studied ZIF materials, and for this reason, we can find much gas sorption data for this adsorbent in the literature. Figure 8 shows the comparison between the adsorption data

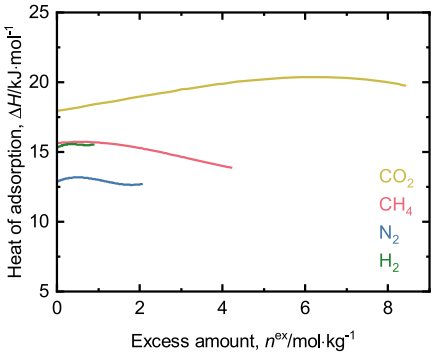

Figure 7. Isosteric heat of adsorption for CO_2, CH_4, N_2, and H_2 plotted as a function of loading.

presented in this study and data sets reported in the literature measured using both gravimetry[44,45,55,56] and volumetry.[37,38,57] We collected literature data from the NIST/ARPA-E Database of Novel and Emerging Adsorbent Materials (https://adsorption.nist.gov/), using the keywords "ZIF-8" for **Adsorbent Material** and "CO2", "CH4", "N2", and "H2" for **Adsorbate Gas**. We restricted the search to experimental measurements taken beyond 1 MPa and within 15 K of the temperature range considered in this study. In addition, we excluded data sets, in which the values obtained from the NIST Database did not match the values reported in the original publication. In total, we identified 3, 4, 2, and 2 studies for CO_2, CH_4, N_2, and H_2, respectively, summarized in Figure 8. The original file names downloaded from the database can be seen in the Supporting Information.

Generally, we observe a good agreement between the data. In particular, the CO_2 adsorption isotherms by Pérez-Pellitero et al.[55] and Xiang et al.[44] agree well with the isotherms reported in this study, accounting for the small difference in the experimental temperatures (Figure 8a). The N_2 adsorption

https://doi.org/10.1021/acs.jced.1c00900
J. Chem. Eng. Data XXXX, XXX, XXX−XXX

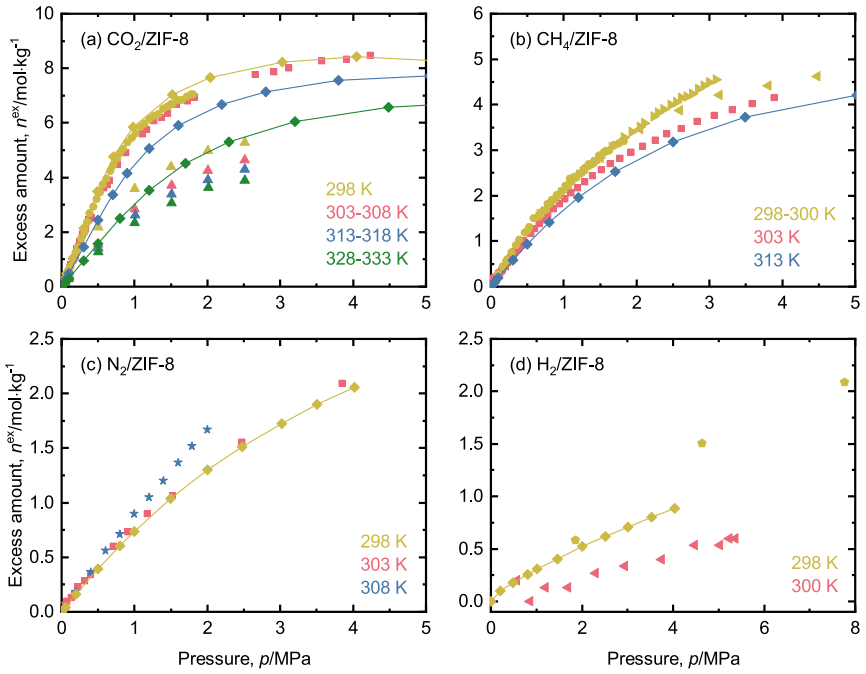

Figure 8. Comparison of the isotherm data reported in this study to the isotherm data published in the literature for (a) CO_2, (b) CH_4, (c) N_2, and (d) H_2. The data sets are from the following references: Pérez-Pellitero et al.[55] (squares), Xiang et al.[44] (circles), Liu et al.[45] (upward triangles), Zhou et al.[37] (left triangles), Mu et al.[57] (right triangles), Parkes et al.[56] (stars), Voskuilen et al.[38] (pentagons), and this study (diamonds connected with lines).

isotherm by Pérez-Pellitero et al.[55] matches well with the isotherm presented in this study although the exothermic nature of adsorption is not well captured (Figure 8c). All the CH_4 isotherms exhibit a good agreement (Figure 8b).

The small disparity among the literature data can arise from multiple factors. For instance, the method of synthesis of ZIF-8 may vary among studies. While we employed a commercial form of ZIF-8, many studies used ZIF-8 synthesized in-house.[37,38,44,45,55] For instance, in the study of Liu et al.[45] that reports lower CO_2 adsorption amounts systematically compared to our work, the synthesized ZIF-8 sample had a lower surface area (1070 m^2/g) and pore volume (0.47 cm^3/g) compared to the values summarized in Table 2. These differences may explain the overall lower CO_2 uptake at all temperatures. Such a discrepancy in the structural properties is prevalent in the literature,[10,43] despite the well-established method of synthesis for ZIF-8. Other factors, such as the value of skeletal density needed to calculate the excess amount of adsorption, may contribute to the observed discrepancies among different studies. As highlighted in this study, relatively small deviations in this parameter (Table 3) result in noticeable differences in the calculated values of the excess adsorption, particularly at high pressure. Unfortunately, this parameter is not always reported in the adsorption studies considered for comparison carried out in Figure 8, precluding a quantification of its contribution to the observed deviations.

Applications. In this section, we make a first appraisal of the potential of ZIF-8 in separations, particularly for the application of separating CO_2 and H_2 in precombustion carbon capture. We do this by looking more generally at the information conveyed by the isotherms gathered in this study. The high CO_2 capacity at high pressures combined with the gentle uptake in the low pressure ranges suggest ZIF-8 may be used in applications such as precombustion carbon capture, where the feed for the separation is supplied at partial pressures that range from 0.4 to 0.7 MPa at a temperature of 308 K.[2] Indeed, ZIF-8 exhibits a lower Henry constant for CO_2 at 308 K than other commercial adsorbents such as zeolite 13X and activated carbon (Norit RB3), as shown in Table 10. The weak adsorbate−adsorbent interactions results in a lower heat of adsorption relative to strong physisorbents, such as zeolite 13X (as seen in Table 10). This implies a stronger temperature dependence of equilibrium adsorption at isobaric conditions of ZIF-8 (as seen in Figure 6), making it a promising material for temperature swing adsorption processes for carbon capture. However, the significantly lower Henry's law selectivity of CO_2 to H_2 for ZIF-8 compared to the other materials indicate a weaker affinity toward CO_2 relative to H_2 at low pressures, suggesting the material may not be viable for the applications with low feed compositions of CO_2.

Table 10. Comparison of ZIF-8 with Zeolite 13X and Activated Carbon[58] in Terms of CO_2 Loading at 0.5 MPa, Henry Constant, Heat of Adsorption at 0.5 MPa and 308 K, and Henry's Law Selectivity at 308 K[a]

parameter	unit	ZIF-8	zeolite 13X	activated carbon
$n^*_{CO_2}$ (0.5 MPa, 308 K)	mol/kg	2.97	4.61	3.73
K_{H,CO_2} (308 K)	mol/kg·MPa	5.2	355.5	22.6
ΔH_{CO_2} (0.5 MPa, 308 K)	kJ/mol	21.39	34.67	22.12
$K_{H,CO_2}/K_{H,H_2}$ (308 K)		19	2400	122

[a]These conditions were chosen for the comparison as they are the typical feed conditions for precombustion carbon capture.[2] The Henry constants and heats of adsorption for zeolite 13X and activated carbon were computed from dual-site Langmuir fitted parameters using the method outlined by Son et al.[59]

As mentioned before, this analysis is a first appraisal of the potential use of ZIF-8 for these applications. For accurate

https://doi.org/10.1021/acs.jced.1c00900
J. Chem. Eng. Data XXXX, XXX, XXX−XXX

prediction of the performance of ZIF-8 in these separations, experimental determination of competitive adsorption of the component gases at the relevant process conditions will be required in addition to the unary adsorption measurements. Other phenomena such as adsorption kinetics and heat transfer in a packed bed will also need to be considered in order to carry out detailed process modeling.

CONCLUSIONS

We have reported gravimetric measurements of adsorption of CO_2, CH_4, N_2, and H_2 in the temperature range of 298.15−393.15 K on ZIF-8 in the pressure range of vacuum to 30 MPa. We presented the adsorption isotherms in their excess format. However, the difficulty of generating reproducible values of skeletal density for highly microporous materials may render the net adsorption isotherms more appropriate for data presentation as the latter definition of adsorption excludes the need to account for the skeletal density. The data reported in this study generally agree well with those reported in the literature. Instances of observed disparity with the literature data may originate from differences in the adsorbent features between the in-house synthesized ZIF-8 used in most previous studies and the commercially obtained ZIF-8 used in this work. The adsorption capacities and the isosteric heat of adsorption indicate a particularly strong adsorption affinity for CO_2, making ZIF-8 a suitable candidate for the applications of gas separations or CO_2 capture.

ASSOCIATED CONTENT

Supporting Information

The Supporting Information is available free of charge at https://pubs.acs.org/doi/10.1021/acs.jced.1c00900.

Supporting figures and tables, uncertainty analysis, NIST/ARPA-E database files, and associated references (PDF)

AUTHOR INFORMATION

Corresponding Author

Camille Petit − *Department of Chemical Engineering, Imperial College London, London SW7 2AZ, United Kingdom;* orcid.org/0000-0002-3722-7984; Email: camille.petit@imperial.ac.uk

Authors

Junyoung Hwang − *Department of Chemical Engineering, Imperial College London, London SW7 2AZ, United Kingdom;* Present Address: Department of Energy Resources Engineering, Stanford University, Stanford, CA 94305, United States

Hassan Azzan − *Department of Chemical Engineering, Imperial College London, London SW7 2AZ, United Kingdom*

Ronny Pini − *Department of Chemical Engineering, Imperial College London, London SW7 2AZ, United Kingdom;* orcid.org/0000-0002-9443-3573

Complete contact information is available at: https://pubs.acs.org/10.1021/acs.jced.1c00900

Notes

The authors declare no competing financial interest.

The current version of the software package used for isotherm fitting and uncertainty calculation is available on the Imperial College London Github repository and can be accessed at https://github.com/ImperialCollegeLondon/IsothermFittingTool. The version of the code used in this publication is referred to by the git commit ID "e3e230a".

ACKNOWLEDGMENTS

J.H. was funded by a departmental scholarship from the Department of Chemical Engineering, Imperial College London. The work was also supported by a donation from Mr. Mark Richardson to the Department of Chemical Engineering at Imperial College London (H.A., R.P., C.P.). The authors acknowledge the technical support of Ms. Giulia Schukraft in conducting the X-ray diffraction pattern analysis of ZIF-8.

REFERENCES

(1) Ruthven, D. M.; Farooq, S.; Knaebel, K. S. *Pressure Swing Adsorption*; VCH: New York, 1994.

(2) Streb, A.; Mazzotti, M. Novel Adsorption Process for Co-Production of Hydrogen and CO_2 from a Multicomponent Stream—Part 2: Application to Steam Methane Reforming and Autothermal Reforming Gases. *Ind. Eng. Chem. Res.* **2020**, *59*, 10093−10109.

(3) Poe, W. A.; Mokhatab, S. *Modeling, Control, and Optimization of Natural Gas Processing Plants*; Elsevier, 2017; Chapter 1, pp 1−72.

(4) Wilkins, N. S.; Rajendran, A. Measurement of competitive CO_2 and N_2 adsorption on Zeolite 13X for post-combustion CO_2 capture. *Adsorption* **2019**, *25*, 115−133.

(5) Hefti, M.; Joss, L.; Bjelobrk, Z.; Mazzotti, M. On the potential of phase-change adsorbents for CO_2 capture by temperature swing adsorption. *Faraday Discuss.* **2016**, *192*, 153−179.

(6) Myers, A. L. Activity coefficients of mixtures adsorbed on heterogeneous surfaces. *AIChE J.* **1983**, *29*, 691−693.

(7) Ritter, J. A.; Bhadra, S. J.; Ebner, A. D. On the Use of the Dual-Process Langmuir Model for Correlating Unary Equilibria and Predicting Mixed-Gas Adsorption Equilibria. *Langmuir* **2011**, *27*, 4700−4712.

(8) García, S.; Pis, J. J.; Rubiera, F.; Pevida, C. Predicting Mixed-Gas Adsorption Equilibria on Activated Carbon for Precombustion CO_2 Capture. *Langmuir* **2013**, *29*, 6042−6052.

(9) Hefti, M.; Marx, D.; Joss, L.; Mazzotti, M. Adsorption equilibrium of binary mixtures of carbon dioxide and nitrogen on zeolites ZSM-5 and 13X. *Microporous Mesoporous Mater.* **2015**, *215*, 215−226.

(10) Park, K. S.; Ni, Z.; Côté, A. P.; Choi, J. Y.; Huang, R.; Uribe-Romo, F. J.; Chae, H. K.; O'Keeffe, M.; Yaghi, O. M. Exceptional chemical and thermal stability of zeolitic imidazolate frameworks. *Proc. Natl. Acad. Sci. U. S. A.* **2006**, *103*, 10186−91.

(11) Tan, J. C.; Bennett, T. D.; Cheetham, A. K. Chemical structure, network topology, and porosity effects on the mechanical properties of Zeolitic Imidazolate Frameworks. *Proc. Natl. Acad. Sci. U. S. A.* **2010**, *107*, 9938−9943.

(12) Rosi, N. L.; Eckert, J.; Eddaoudi, M.; Vodak, D. T.; Kim, J.; O'Keeffe, M.; Yaghi, O. M. Hydrogen Storage in Microporous Metal-Organic Frameworks. *Science* **2003**, *300*, 1127−1129.

(13) Banerjee, R.; Phan, A.; Wang, B.; Knobler, C.; Furukawa, H.; O'Keeffe, M.; Yaghi, O. M. High-Throughput Synthesis of Zeolitic Imidazolate Frameworks and Application to CO_2 Capture. *Science* **2008**, *319*, 939−943.

(14) Hu, Y.; Liu, Z.; Xu, J.; Huang, Y.; Song, Y. Evidence of pressure enhanced CO_2 storage in ZIF-8 probed by FTIR spectroscopy. *J. Am. Chem. Soc.* **2013**, *135*, 9287−9290.

(15) Zhang, K.; Lively, R. P.; Zhang, C.; Chance, R. R.; Koros, W. J.; Sholl, D. S.; Nair, S. Exploring the Framework Hydrophobicity and Flexibility of ZIF-8: From Biofuel Recovery to Hydrocarbon Separations. *J. Phys. Chem. Lett.* **2013**, *4*, 3618−3622.

(16) Danaci, D.; Singh, R.; Xiao, P.; Webley, P. A. Assessment of ZIF materials for CO_2 capture from high pressure natural gas streams. *Chem. Eng. J.* **2015**, *280*, 486−493.
(17) Li, W.; Wu, X.; Liu, H.; Chen, J.; Tang, W.; Chen, Y. Hierarchical hollow ZnO cubes constructed using self-sacrificial ZIF-8 frameworks and their enhanced benzene gas-sensing properties. *New J. Chem.* **2015**, *39*, 7060−7065.
(18) Liu, S.; Sun, L.-X.; Zhou, Y.-L.; Liu, L.-T. Heat capacities and thermodynamic properties of a Zn-based zeolitic imidazolate framework. *J. Therm. Anal. Calorim.* **2019**, *135*, 3191−3196.
(19) Davoodian, N.; Nakhaei Pour, A.; Izadyar, M.; Mohammadi, A.; Salimi, A.; Kamali Shahri, S. M. Fischer−Tropsch synthesis using zeolitic imidazolate framework (ZIF-7 and ZIF-8)-supported cobalt catalysts. *Appl. Organomet. Chem.* **2020**, *34*, 1−10.
(20) Hwang, J.; Pini, R. Supercritical CO_2 and CH_4 Uptake by Illite-Smectite Clay Minerals. *Environ. Sci. Technol.* **2019**, *53*, 11588−11596.
(21) Leachman, J. W.; Jacobsen, R. T.; Penoncello, S. G.; Lemmon, E. W. Fundamental Equations of State for Parahydrogen, Normal Hydrogen, and Orthohydrogen. *J. Phys. Chem. Ref. Data* **2009**, *38*, 721−748.
(22) Lemmon, E. W.; Bell, I. H.; Huber, M. L.; McLinden, M. O. *NIST Standard Reference Database 23: Reference Fluid Thermodynamic and Transport Properties-REFPROP*; 2018; https://www.nist.gov/srd/refprop.
(23) Pini, R.; Ansari, H.; Hwang, J. Measurement and interpretation of unary supercritical gas adsorption isotherms in micro-mesoporous solids. *Adsorption* **2021**, *27*, 659.
(24) Han, R.; Walton, K. S.; Sholl, D. S. Does Chemical Engineering Research Have a Reproducibility Problem? *Annu. Rev. Chem. Biomol. Eng.* **2019**, *10*, 43−57.
(25) Nguyen, H. G. T.; Espinal, L.; van Zee, R. D.; Thommes, M.; Toman, B.; Hudson, M. S. L.; Mangano, E.; Brandani, S.; Broom, D. P.; Benham, M. J.; Cychosz, K. A.; Bertier, P.; Yang, F.; Krooss, B. M.; Siegelman, R. L.; Hakuman, M.; Nakai, K.; Ebner, A. D.; Erden, L.; Ritter, J. A.; Moran, A.; Talu, O.; Huang, Y.; Walton, K. S.; Billemont, P.; De Weireld, G. A reference high-pressure CO_2 adsorption isotherm for ammonium ZSM-5 zeolite: results of an interlaboratory study. *Adsorption* **2018**, *24*, 531−539.
(26) Nguyen, H. G. T.; Sims, C. M.; Toman, B.; Horn, J.; van Zee, R. D.; Thommes, M.; Ahmad, R.; Denayer, J. F. M.; Baron, G. V.; Napolitano, E.; Bielewski, M.; Mangano, E.; Brandani, S.; Broom, D. P.; Benham, M. J.; Dailly, A.; Dreisbach, F.; Edubilli, S.; Gumma, S.; Möllmer, J.; Lange, M.; Tian, M.; Mays, T. J.; Shigeoka, T.; Yamakita, S.; Hakuman, M.; Nakada, Y.; Nakai, K.; Hwang, J.; Pini, R.; Jiang, H.; Ebner, A. D.; Nicholson, M. A.; Ritter, J. A.; Farrando-Pérez, J.; Cuadrado-Collados, C.; Silvestre-Albero, J.; Tampaxis, C.; Steriotis, T.; Řimnáčová, D.; Švábová, M.; Vorokhta, M.; Wang, H.; Bovens, E.; Heymans, N.; De Weireld, G. A reference high-pressure CH_4 adsorption isotherm for zeolite Y: results of an interlaboratory study. *Adsorption* **2020**, *26*, 1253−1266.
(27) Rouquerol, F.; Rouquerol, J.; Sing, K. S. W.; Llewellyn, P.; Maurin, G. *Adsorption by Powders and Porous Solids: Principles, Methodology and Applications*, 2nd ed.; Academic Press: Oxford, 2014.
(28) Bard, Y. *Nonlinear Parameter Estimation*; Academic Press: New York, 1973.
(29) Myers, A. L. In *Chemical Thermodynamics for Industry*; Letcher, T. M., Ed.; Royal Society of Chemistry, 2004; Chapter 21, pp 243−253.
(30) Czepirski, L.; Jagiello, J. Virial-type thermal equation of gas-solid adsorption. *Chem. Eng. Sci.* **1989**, *44*, 797−801.
(31) Nuhnen, A.; Janiak, C. A practical guide to calculate the isosteric heat/enthalpy of adsorption via adsorption isotherms in metal−organic frameworks, MOFs. *Dalton Trans* **2020**, *49*, 10295−10307.
(32) Malbrunot, P.; Vidal, D.; Vermesse, J.; Chahine, R.; Bose, T. K. Adsorbent Helium Density Measurement and Its Effect on Adsorption Isotherms at High Pressure. *Langmuir* **1997**, *13*, 539−544.
(33) Do, D. D.; Do, H. D. Appropriate volumes for adsorption isotherm studies: The absolute void volume, accessible pore volume and enclosing particle volume. *J. Colloid Interface Sci.* **2007**, *316*, 317−330.
(34) Do, D. D.; Do, H. D.; Fan, C.; Nicholson, D. On the Existence of Negative Excess Isotherms for Argon Adsorption on Graphite Surfaces and in Graphitic Pores under Supercritical Conditions at Pressures up to 10,000 atm. *Langmuir* **2010**, *26*, 4796−4806.
(35) Brandani, S.; Mangano, E.; Sarkisov, L. Net, excess and absolute adsorption and adsorption of helium. *Adsorption* **2016**, *22*, 261−276.
(36) Nguyen, H. G. T.; Horn, J. C.; Bleakney, M.; Siderius, D. W.; Espinal, L. Understanding Material Characteristics through Signature Traits from Helium Pycnometry. *Langmuir* **2019**, *35*, 2115−2122.
(37) Zhou, W.; Wu, H.; Hartman, M. R.; Yildirim, T. Hydrogen and methane adsorption in Metal-Organic Frameworks: a high-pressure volumetric study. *J. Phys. Chem. C* **2007**, *111*, 16131−16137.
(38) Voskuilen, T. G.; Pourpoint, T. L.; Dailly, A. M. Hydrogen adsorption on microporous materials at ambient temperatures and pressures up to 50 MPa. *Adsorption* **2012**, *18*, 239−249.
(39) Thommes, M.; Kaneko, K.; Neimark, A. V.; Olivier, J. P.; Rodriguez-Reinoso, F.; Rouquerol, J.; Sing, K. S. W. Physisorption of gases, with special reference to the evaluation of surface area and pore size distribution (IUPAC Technical Report). *Pure Appl. Chem.* **2015**, *87*, 1051−1069.
(40) Fairen-Jimenez, D.; Moggach, S. A.; Wharmby, M. T.; Wright, P. A.; Parsons, S.; Düren, T. Opening the Gate: Framework Flexibility in ZIF-8 Explored by Experiments and Simulations. *J. Am. Chem. Soc.* **2011**, *133*, 8900−8902.
(41) Casco, M. E.; Cheng, Y. Q.; Daemen, L. L.; Fairen-Jimenez, D.; Ramos-Fernández, E. V.; Ramirez-Cuesta, A. J.; Silvestre-Albero, J. Gate-opening effect in ZIF-8: the first experimental proof using inelastic neutron scattering. *Chem. Commun.* **2016**, *52*, 3639−3642.
(42) Casco, M. E.; Fernández-Catalá, J.; Cheng, Y.; Daemen, L.; Ramirez-Cuesta, A. J.; Cuadrado-Collados, C.; Silvestre-Albero, J.; Ramos-Fernandez, E. V. Understanding ZIF-8 Performance upon Gas Adsorption by Means of Inelastic Neutron Scattering. *ChemistrySelect* **2017**, *2*, 2750−2753.
(43) Cravillon, J.; Münzer, S.; Lohmeier, S.-J.; Feldhoff, A.; Huber, K.; Wiebcke, M. Rapid Room-Temperature Synthesis and Characterization of Nanocrystals of a Prototypical Zeolitic Imidazolate Framework. *Chem. Mater.* **2009**, *21*, 1410−1412.
(44) Xiang, Z.; Peng, X.; Cheng, X.; Li, X.; Cao, D. CNT@$Cu_3(BTC)_2$ and Metal−Organic Frameworks for Separation of CO_2/CH_4 Mixture. *J. Phys. Chem. C* **2011**, *115*, 19864−19871.
(45) Liu, D.; Wu, Y.; Xia, Q.; Li, Z.; Xi, H. Experimental and molecular simulation studies of CO_2 adsorption on zeolitic imidazolate frameworks: ZIF-8 and amine-modified ZIF-8. *Adsorption* **2013**, *19*, 25−37.
(46) Di Giovanni, O.; Dörfler, W.; Mazzotti, M.; Morbidelli, M. Adsorption of supercritical carbon dioxide on silica. *Langmuir* **2001**, *17*, 4316−4321.
(47) Moellmer, J.; Moeller, A.; Dreisbach, F.; Glaeser, R.; Staudt, R. High pressure adsorption of hydrogen, nitrogen, carbon dioxide and methane on the metal-organic framework HKUST-1. *Microporous Mesoporous Mater.* **2011**, *138*, 140−148.
(48) Zeng, Q.; Wang, Z.; Sui, T.; Huang, T. Adsorption Mechanisms of High-Pressure Methane and Carbon Dioxide on Coals. *Energy Fuels* **2021**, *35*, 13011−13021.
(49) Schell, J.; Casas, N.; Pini, R.; Mazzotti, M. Pure and binary adsorption of CO_2, H_2, and N_2 on activated carbon. *Adsorption* **2012**, *18*, 49−65.
(50) Hwang, J.; Joss, L.; Pini, R. Measuring and modelling supercritical adsorption of CO_2 and CH_4 on montmorillonite source clay. *Microporous Mesoporous Mater.* **2019**, *273*, 107−121.
(51) Lemmon, E. W.; McLinden, M. O.; Friend, D. G. *Thermophysical Properties of Fluid Systems*. 1998; https://webbook.nist.gov/chemistry/.
(52) Yang, J.; Ren, Y.; Tian, A.-m.; Sun, H. COMPASS Force Field for 14 Inorganic Molecules, He, Ne, Ar, Kr, Xe, H_2, O_2, N_2, NO, CO,

https://doi.org/10.1021/acs.jced.1c00900
J. Chem. Eng. Data XXXX, XXX, XXX−XXX

CO_2, NO_2, CS_2, and SO_2, in Liquid Phases. *J. Phys. Chem. B* **2000**, *104*, 4951−4957.
(53) Ruthven, D. M. *Adsorption*; 2000.
(54) Ruthven, D. M. *Principles of Adsorption and Adsorption Processes*; John Wiley and Sons: New York, 1984.
(55) Pérez-Pellitero, J.; Amrouche, H.; Siperstein, F. R.; Pirngruber, G.; Nieto-Draghi, C.; Chaplais, G.; Simon-Masseron, A.; Bazer-Bachi, D.; Peralta, D.; Bats, N. Adsorption of CO_2, CH_4, and N_2 on zeolitic imidazolate frameworks: experiments and simulations. *Chem. - Eur. J.* **2010**, *16*, 1560−1571.
(56) Parkes, M. V.; Staiger, C. L.; Perry IV, J. J.; Allendorf, M. D.; Greathouse, J. A. Screening metal−organic frameworks for selective noble gas adsorption in air: effect of pore size and framework topology. *Phys. Chem. Chem. Phys.* **2013**, *15*, 9093.
(57) Mu, L.; Liu, B.; Liu, H.; Yang, Y.; Sun, C.; Chen, G. A novel method to improve the gas storage capacity of ZIF-8. *J. Mater. Chem.* **2012**, *22*, 12246.
(58) Delgado, J. A.; Águeda, V. I.; Uguina, M. A.; Sotelo, J. L.; Brea, P.; Grande, C. A. Adsorption and Diffusion of H_2, CO, CH_4, and CO_2 in BPL Activated Carbon and 13X Zeolite: Evaluation of Performance in Pressure Swing Adsorption Hydrogen Purification by Simulation. *Ind. Eng. Chem. Res.* **2014**, *53*, 15414−15426.
(59) Son, K. N.; Cmarik, G. E.; Knox, J. C.; Weibel, J. A.; Garimella, S. V. Measurement and Prediction of the Heat of Adsorption and Equilibrium Concentration of CO_2 on Zeolite 13X. *J. Chem. Eng. Data* **2018**, *63*, 1663−1674.

https://doi.org/10.1021/acs.jced.1c00900
J. Chem. Eng. Data XXXX, XXX, XXX−XXX